Weak localization and mobility in ZnO nanostructures

Edward M. Likovich,* Kasey J. Russell, Eric W. Petersen, and Venkatesh Narayanamurti
School of Engineering and Applied Sciences, Harvard University, Cambridge, Massachusetts 02138, USA
(Received 19 August 2009; revised manuscript received 21 October 2009; published 18 December 2009)

We conduct a comprehensive investigation into the electronic and magnetotransport properties of ZnO nanoplates grown concurrently with ZnO nanowires by the vapor-liquid-solid method. We present magnetoresistance data showing weak localization in our nanoplates and probe its dependence on temperature and carrier concentration. We measure phase coherence lengths of 50–100 nm at 1.9 K and, because we do not observe spin-orbit scattering through antilocalization, suggest that ZnO nanostructures may be promising for further spintronic study. We then proceed to study the effect of weak localization on electron mobility using four-terminal van der Pauw resistivity and Hall measurements versus temperature and carrier concentration. We report an electron mobility of $\sim 100\ \mathrm{cm^2/V\ s}$ at 275 K, comparable to what is observed in ZnO thin films. We compare Hall mobility to field-effect mobility, which is more commonly reported in studies on ZnO nanowires and find that field-effect mobility tends to overestimate Hall mobility by a factor of 2 in our devices. Finally, we comment on temperature-dependent hysteresis observed during transconductance measurements and its relationship to mobile, positively charged Zn interstitial impurities.

DOI: 10.1103/PhysRevB.80.245318 PACS number(s): 73.63.−b

I. INTRODUCTION

ZnO has been extensively studied due to its favorable optoelectronic properties which include a wide band gap (3.37 eV), strong exciton binding energy (60 meV), and potential use as a transparent conductor in light-emitting and light-collecting devices.[1–3] *p*-type doping of ZnO has recently been demonstrated in both bulk films[4,5] and nanowires,[6] opening the door for a variety of devices based on *p*-*n* junctions. Additionally, ZnO nanowires have shown promise in applications that include gas sensors, which take advantage of their high surface area to volume ratio[7] and room-temperature spintronics, as the incorporation of transition metals has been shown to induce ferromagnetism in both bulk ZnO (Ref. 8) and ZnO nanowires.[9,10] ZnO nanowires have also demonstrated amplified spontaneous emission[11] and room-temperature UV lasing due to their high exciton binding energy.[12] For a review of ZnO device applications, see Ref. 13.

Much recent research has focused on spin injection and transport in semiconductors, potentially leading the way to a new paradigm of electronics based on spin.[14–16] The interest of spin-dependent transport has extended to ZnO thin films doped with Mn, which have shown interesting spin-orbit and *s*-*d* exchange interactions.[17] However, there has not been a significant investigation of magnetotransport in ZnO nanostructures, despite a wide interest in nanostructure devices.

In this paper we report on the electronic and magnetotransport properties of ZnO nanoplates, structures as thin as typical ZnO nanowires (~ 100 nm) but several microns long and wide, that are grown simultaneously alongside nanowires by the vapor-liquid-solid (VLS) method. The nanoplate geometry, in contrast to that of a nanowire, allows us to make four-wire Hall and van der Pauw resistivity measurements. We believe our results generally apply to ZnO nanowires as well since they are also expected to exhibit three-dimensional electron-transport properties as the diameters of typical ZnO nanowires (30–100 nm) are insufficiently small to establish quantum confinement in the radial direction.[18]

We present data characteristic of weak localization in ZnO nanostructures and probe its dependence on temperature and carrier concentration. From this we are able to determine the inelastic-scattering lifetime of electrons and, due to an absence of antilocalization, believe that the spin-orbit scattering lifetime is significantly longer than the inelastic-scattering lifetime. We then consider how weak localization affects mobility and carrier transport by conducting Hall measurements for different temperatures and carrier concentrations. We compare these values with the two-terminal field-effect approximation commonly reported in the literature but which suffer from parasitic contact resistance and rely on assumptions about the geometric extent of the nanowire conduction channel.[19–22] Recent work suggests that there may be independent core and surface conduction mechanisms,[23] which would need to be taken into consideration to accurately determine the field-effect or effective mobility. Finally, we comment on temperature-dependent hysteresis observed during transconductance measurements and its possible relationship to mobile, charged impurities.

II. FABRICATION AND EXPERIMENTAL SETUP

We fabricated ZnO nanoplates using the VLS growth mechanism, first demonstrated by Wagner and Ellis.[24] The growth apparatus used for this experiment consisted of a single-zone tube furnace (from Lindberg/Blue) through which we passed a metered flow of Ar and O_2 in a 1000:1 ratio. A quartz sample holder, containing both the Si(111) substrate (with 5 nm diameter Au catalyst nanoparticles dispersed onto it) and a mixture of ZnO powder and graphite (1:1 ratio by volume), was used to move the substrate in and out of the hot zone of the furnace, thereby initiating and terminating nanowire growth. After a growth of 45 min at 975 °C, ZnO nanowires and nanoplates were present on the substrate. The nanoplates had gold catalyst particles at their

 ©2009 The American Physical Society

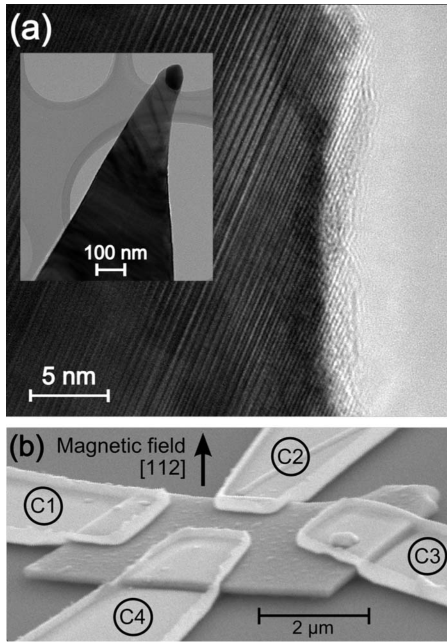

FIG. 1. (a) TEM atomic-resolution image showing the crystalline nature of our nanoplates. (Inset) TEM image taken at lower magnification showing the Au catalyst at the end of the nanoplate, which is characteristic of vapor-liquid-solid growth. (b) Scanning electron microscopy image of a ZnO nanoplate device. The four contacts are labeled C1, C2, C3, and C4. A 300 nm SiO_2 layer serves as the gate barrier with the gate contact to the backside of the heavily doped Si substrate.

tip (characteristic of VLS growth) and were single crystalline, as shown in Fig. 1(a). Atomic force microscopy and scanning electron microscopy analysis indicated that the nanoplates were roughly the same thickness as typical nanowires (~100 nm) but extended several microns laterally, as shown in Fig. 1(b). The growth of similar nanoplates has been reported in the literature for both VLS (Ref. 25) and solution synthesis[26] methods. We offer the additional observation that ZnO nanoplates tend to preferentially grow on substrates that form a native oxide layer; we observed them on both Si(111) and Ti foil substrates, but not on Mo foil.[27]

To experimentally probe the nanoplates, we first removed them from the substrate by sonication in isopropanol for short bursts of several seconds. This created an isopropanol solution containing suspended nanoplates. We then used a pipette to deposit droplets of the solution onto a p++ Si wafer with a 300 nm thermally grown oxide layer. We allowed the droplet to air dry, recorded the positions of the deposited nanostructures, and used electron-beam lithography to define four contacts (sputtered 20 nm Ti, followed by 80 nm Au) to each nanoplate, as shown in Fig. 1(b). These contact metals resulted in ohmic behavior at the biases measured and are commonly used in the literature.[28,29] An In back contact was cold pressed to the Si substrate to control carrier concentration through gating. The devices were then placed in a variable-temperature cryostat capable of applying a magnetic field perpendicular to the surface of the device, which was identified as the [112] direction by transmission electron microscopy (TEM) diffraction patterns. A total of eight devices were measured, all of which exhibited similar behavior.

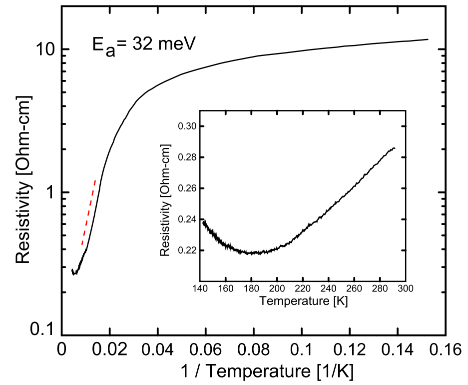

FIG. 2. (Color online) Semi-log plot of van der Pauw resistivity versus $1/T$. The resistivity exhibits an exponential dependence in $1/T$ and we observe a distinct activation energy of 32 meV that corresponds to Zn interstitials. The red, dashed line is meant to guide the eye to the linear region from which activation energy is extracted. (Inset) High temperature van der Pauw resistivity showing an absolute minimum near 180 K, above which resistivity scales linearly with T, characteristic of electron-phonon scattering.

III. RESISTIVITY

As the devices were cooled, we measured resistivity as a function of temperature using the van der Pauw formulation, which enables the resistivity of a planar sample of arbitrary shape to be determined with corrections for contact anisotropy.[30,31] To do so, we sourced a sinusoidal signal of 30 nA rms between contacts C1 and C2 (see Fig. 1) and concurrently measured voltage between contacts C3 and C4 with a lock-in amplifier. Immediately following this, contacts C1 and C4 were swapped and a second measurement was taken such that current was sourced between contacts C2 and C3 and voltage was concurrently measured between contacts C4 and C1.

As shown in Fig. 2, resistivity increases linearly with T at high temperatures (200–300 K), as expected for phonon-dominated scattering. For low temperatures (below 150 K), resistivity scales exponentially in $1/T$, characteristic of a lightly doped semiconductor.[32] We observed a minimum resistivity around 180 K, which has been reported in the ZnO literature and likely represents the point at which the additive resistive contributions of phonon scattering and electron weak localization are at a minimum.[33,34] A discussion of electron weak localization, which opposes diffusive transport at low temperatures, is covered extensively in the next section.

We observed a distinct activation energy characterized by the linear region in the semi-log plot of resistivity shown in Fig. 2. The activation energy was obtained by fitting the data to an exponential functional form in the limit of no compensation, $\exp(-E_a/2kT)$, where E_a is the activation energy; k is the Boltzmann constant; and T is the temperature. From this analysis, we calculate E_a=32 meV. This 32 meV activation energy is consistent with reports in the literature for Zn interstitials, which act as electron donors.[35]

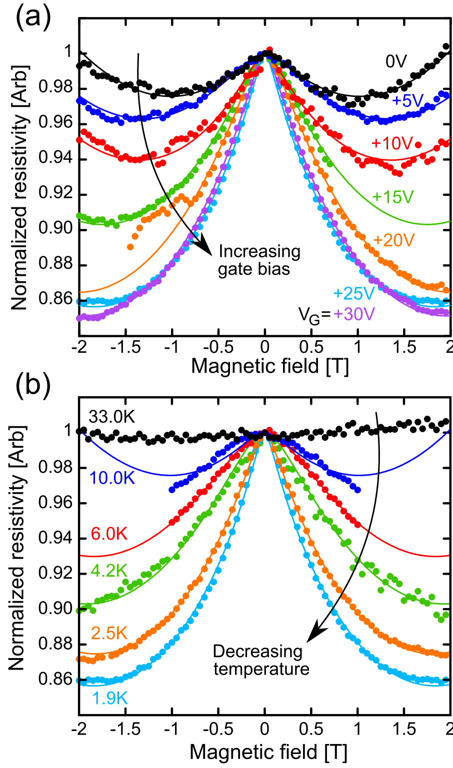

FIG. 3. (Color online) Magnetoresistance measurements of weak localization. (a) A series of gate biases (and thus carrier densities) at constant temperature (1.9 K). Experimental data are plotted as colored circles, with solid lines corresponding to fits to Eq. (1). The corresponding carrier concentrations range from 1.1×10^{17} cm^{-3} for V_G=0 V to 7.4×10^{17} cm^{-3} for V_G=+30 V. (b) A series of temperatures at constant gate bias (V_G=+30 V). The effect is destroyed for high temperatures due to loss of phase coherence from increased inelastic scattering.

IV. WEAK LOCALIZATION

Electron weak localization originates from the constructive interference of backscattered electronic wave functions which increases the probability of localizing an electron. This phenomenon manifests itself by a positive correction to resistivity at zero magnetic field, which is easily broken by applying a magnetic field to destroy coherent superposition. For a more thorough review of weak localization, see Refs. 36 and 37.

We observed weak localization as a positive correction to van der Pauw resistivity at zero magnetic field for a variety of carrier concentrations and temperatures as presented in Fig. 3 [see Fig. 1(b) for experimental setup]. As expected, the effect was temperature dependent and was strongest at low temperatures (10 K and below), with a very small effect at 16 K and no effect at 33 K. The effect dies out for higher temperatures because the inelastic-scattering lifetime, τ, becomes comparable to the elastic-scattering lifetime, at which point the phase coherence necessary for weak localization is destroyed. We also found the effect to be dependent on carrier concentration, with higher carrier concentrations yielding larger corrections to resistivity. We attribute this to the larger fractional change in resistivity, $\Delta\rho/\rho$, caused by the reduction in absolute resistivity, ρ, accompanying higher carrier concentrations. The observed increase in τ with carrier density agrees with reports of weak localization in Si metal-oxide-semiconductor field-effect transistors.[38]

The observation of weak localization has been reported in the literature for ZnO thin films doped with Al,[39] B,[33] and transition metals[40] but not yet in ZnO nanostructures. Contrary to Refs. 39 and 40, we observe no evidence of antilocalization (a negative correction to resistivity at zero magnetic field caused by spin-orbit scattering) for temperatures as low as 1.9 K. This suggests that the spin-orbit scattering lifetime is significantly longer than the inelastic-scattering lifetime in natively doped ZnO nanostructures.

The theory behind weak localization is readily found in the literature for both two-dimensional[41] and three-dimensional[42,43] systems. Because of their size, we expect our nanoplates to exhibit three-dimensional transport and as we will show, the theory of weak localization in three dimensions provides an excellent description of the transport that we observe. For three-dimensional systems, the correction to resistivity, $\Delta\rho/\rho$, scales as B^2 for small magnetic fields and as $B^{1/2}$ for large magnetic fields, according to

$$\frac{\Delta\rho}{\rho} = -\alpha\rho\frac{e^2}{2\pi^2\hbar}\sqrt{\frac{eB}{\hbar}}F(x), \tag{1}$$

where $\frac{\Delta\rho}{\rho}$ is the fractional change in resistivity due to applied magnetic field; α is a coefficient between 0 and 1 that is thought to represent Coulomb screening; ρ is the resistivity; e is the electronic charge; $\hbar$ is Planck's constant; B is the applied magnetic field; and $F(x)$ is a Hurwitz zeta function given by

$$F(x) = \sum_{n=0}^{\infty}[2(n+1+1/x)^{1/2} - 2(n+1/x)^{1/2} - (n+1/2 + 1/x)^{-1/2}], \tag{2}$$

where x is a dimensionless quantity defined by $x = 4eD\tau B/\hbar$; D is the electron diffusion constant; and τ is the electron inelastic-scattering lifetime. We analyzed our data in a similar manner to that of Ref. 44 and used a nonlinear least-squares method to fit the data using two free parameters, α and τ. For high magnetic fields, a positive dependence on B^2 was observed and is characteristic of the usual quadratic magnetoresistance observed in bulk semiconductors.[44] We accounted for this by including a temperature-independent quadratic term, obtained by fitting to high-temperature data. Error bars in Fig. 4 indicate the 95% confidence intervals of the fits.

As shown in Fig. 4(a), calculated inelastic-scattering lifetimes scale with temperature as T^{-3}, characteristic of inelastic scattering by electron-phonon processes.[45] There was only a slight observed dependence on carrier concentration (gate bias); the inelastic-scattering lifetime was 5.7 ± 0.4 ns at a carrier concentration of 7.4×10^{17} cm^{-3} at 1.9 K compared to 3.0 ± 0.8 ns at a carrier concentration of 1.3×10^{17} cm^{-3} at 1.9 K. Additionally, we calculate the phase coherence length, $\ell_\phi = \sqrt{D\tau}$, which is plotted versus temperature in Fig. 4(b). Here, we see temperature dependence that

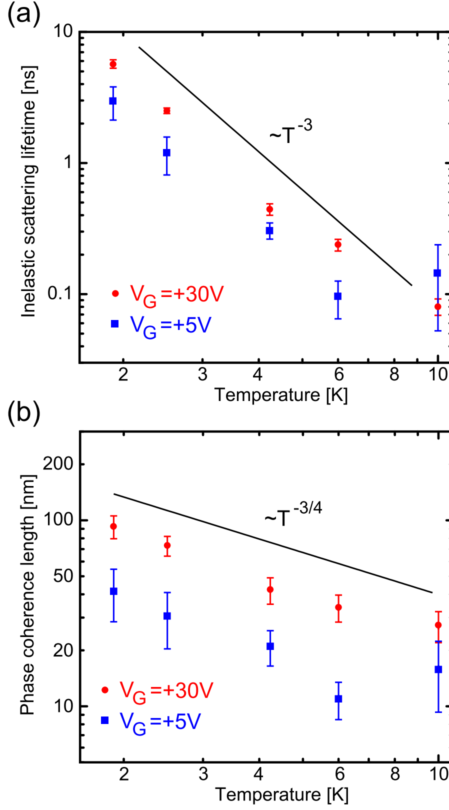

FIG. 4. (Color online) (a) Electron inelastic-scattering lifetime versus temperature for V_G=+30 V (red circles) and V_G=0 V (blue squares). The line is meant to guide the eye to a T^{-3} dependence, characteristic of electron-phonon scattering. (b) Electron phase coherence length versus temperature plotted for V_G=+30 V (red circles) and V_G=0 V (blue squares). The line is meant to guide the eye to a $T^{-3/4}$ dependence, which has also been observed in ZnO thin films.

scales as $T^{-3/4}$, the same behavior that was reported for doped ZnO thin films in Ref. 39. Although our material is not degenerately doped, we must still use the generalized form of the Einstein relation to analyze the temperature dependence of D at the low temperatures reported in Fig. 4.[46] This is because the carrier density in our sample is controlled by the gate bias and does not vary with temperature in this temperature range. The temperature dependence of D is therefore simply proportional to that of μ, which should scale as $T^{3/2}$ in the impurity-dominated regime.[47] We therefore expect $\ell_\phi \sim T^{-3/4}$, consistent with the observed behavior.

Measured phase coherence lengths range from 27 ± 5 nm at 10 K to 93 ± 13 nm at 1.9 K for V_G=+30 V. These values are roughly an order of magnitude lower than the report on heavily doped ZnO thin films in Ref. 39; we believe this to be a result of their significantly larger carrier concentration (10^{20} cm^{-3} compared to 10^{17} cm^{-3} in our device) that effectively screens charged impurities. Our results suggest that ZnO may be useful for spintronic studies, given that we observe coherence lengths of 10–100 nm and no evidence of spin-orbit scattering through antilocalization.

V. HALL MOBILITY MEASUREMENTS

Hall mobility measurements were conducted as a function of both temperature and carrier concentration. Devices were measured in a typical Hall configuration: a sinusoidal signal of 30 nA rms was sourced between contacts C2 and C4, and the Hall voltage was concurrently measured between contacts C1 and C3 [see Fig. 1(b)] while sweeping the perpendicular magnetic field. Temperature was varied from 1.9 to 275 K and carrier concentration was modulated by applying a gate bias to the p++ Si substrate relative to the current sink, C4. Gate bias was applied in 5 V steps from 0 V to +30 V, corresponding to carrier densities between 1.1×10^{17} and 7.4×10^{17} cm^{-3} at 1.9 K and between 8.6×10^{17} and 1.5×10^{18} cm^{-3} at 275 K. We infer that our devices are n-type doped by observing an increase in conductivity for a positive applied gate bias.

Using the change in Hall voltage versus magnetic field, we calculate Hall mobility[31] and plot it as a function of both temperature and carrier concentration in Fig. 5. We report a Hall mobility of 103 ± 5 cm^2/V s for 0 V gate bias at 275 K. By increasing gate bias to +30 V at 275 K, the mobility increases to 131 cm^2/V s. These values are comparable to those reported in the literature for ZnO thin films grown on sapphire by pulsed laser deposition[48] and molecular beam epitaxy[49,50] but are an order of magnitude larger than those reported on ZnO nanowires,[21,34] with the exception of nanowires with surface passivation treatments that have field-effect mobilities above 1000 cm^2/V s.[22]

As temperature decreases, electron mobility first increases due to reduced electron-phonon scattering, reaches a peak and then decreases to the lowest temperature we measured, 1.9 K, where we report a mobility of 31 ± 10 cm^2/V s at 0 V gate bias and 92 ± 2 cm^2/V s at +30 V gate bias. The effect of carrier concentration on mobility is significantly increased at lower temperatures; this may be the result of increased electron screening which reduces the effect of charged impurity scattering.[51] Similar behavior is also reported for ZnO thin films in the literature, with a mobility peak occurring near 110 K.[52] The temperature dependence of mobility appears to scale more slowly than the $T^{3/2}$ expected for impurity scattering in ZnO bulk crystals at low temperature.[53–55] This scaling difference may be the result of a few factors, including weak localization suppressing mobility, a significant dependence on carrier density that affects impurity screening, or mobile, charged impurities which are described in Sec. VI. Although further investigation is needed to conclusively understand this temperature dependence, we suspect a significant contribution from the mobile impurities, as measurements were very sensitive to thermal cycling.

Nanoplates provide a useful platform to compare Hall mobility with the typically reported field-effect and effective mobilities in nanowires[21,34] because our four-wire contact geometry allows us to measure all three mobilities on the same nanoplate device. The more commonly reported field-effect mobility is calculated with a two-terminal transconductance measurement according to Ref. 31,

$$\mu_{FE} = \frac{L}{W}\frac{g_m}{C_{ox}V_{DS}}, \quad (3)$$

where L/W is the ratio of channel length to channel width; g_m is the transconductance; C_{ox} is the oxide capacitance per

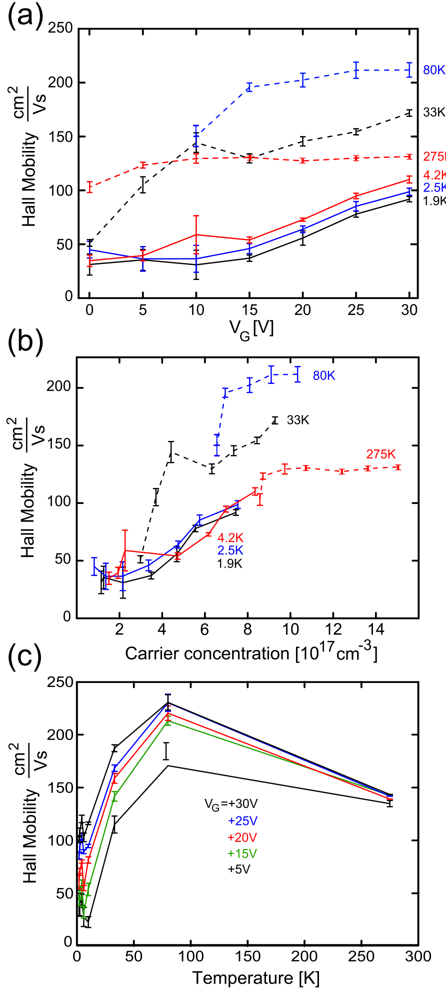

FIG. 5. (Color online) (a) Hall mobility versus gate bias for temperatures ranging from 1.9 to 275 K. Mobility exhibits a larger dependence on carrier concentration at low temperature, where higher carrier density increases mobility. (b) Hall mobility versus carrier concentration. Mobility increases roughly linearly with carrier concentration and appears to saturate at higher carrier densities. (c) Hall mobility versus temperature. Mobility increases with temperature, reaches a maximum, and then decreases, consistent with previous reports on ZnO thin films.

unit area; and V_{DS} is the drain-source bias. In our device, we geometrically measure $L/W=2.71$ and C_{ox} is calculated for a 300-nm-thick SiO_2 layer to be 11 500 pF/cm^2. We experimentally determine transconductance by applying a small dc source-drain bias, V_{DS}, across contacts C2 and C4 and measure current while varying gate bias.

The effective mobility, as with the field-effect mobility, is determined using only a two-terminal measurement. Instead of estimating the mobility from the transconductance of the device, the source-drain conductance is used[31]

$$\mu_{EFF} = \frac{L}{W}\frac{g_d}{C_{ox}(V_G - V_T)}, \tag{4}$$

where L/W is the ratio of channel length to channel width; g_d is the drain conductance; C_{ox} is the oxide capacitance per unit area; V_G is the gate bias; and V_T is the turn-on threshold.

The preference for Hall mobility is clear because it has no dependence on sample geometry. Additionally, Hall mobility is able to be determined independently from the carrier concentration. In contrast, field-effect mobility is limited to the gate bias at which the region of linear transconductance occurs. Effective mobility has the added complication that it also depends on the threshold voltage, which we show to be highly influenced by mobile impurities in the next section.

Comparing the Hall mobility to field-effect mobility for the temperatures and carrier concentrations measured here, we conclude that the field-effect approximation tends to overestimate Hall mobility by about a factor of 2 in our devices. Field-effect mobility does report the correct order of magnitude, so it can be a useful approximation when a precise value is not necessary. Additionally, field-effect mobility provides no indication of the temperature-dependent mobility peak shown in Fig. 5(c) and reported in the literature. We believe this to be an inherent limitation of the field-effect measurement since it cannot determine mobility independent of carrier concentration.

VI. THRESHOLD BEHAVIOR

During transconductance measurements at high temperatures (100 K and above), hysteresis was observed between successive sweeps, as shown in Fig. 6(a). This hysteresis is well documented in the literature, with both surface adsorption[34,56] and mobile impurities[57,58] cited as possible mechanisms. Additionally, we observed that the threshold voltage can be varied over tens of volts by holding the gate at high or low bias for a period of time, as shown in Fig. 6(b). We note that the threshold voltage always moves toward the gate bias, that is, for V_G=+30 V the threshold would move toward +30 V and for V_G=−30 V the threshold would move toward −30 V.

Our experimental data suggest that this hysteresis is the result of mobile Zn interstitials within the ZnO nanoplate. We believe this for several reasons: (1) the literature reports that Zn interstitials become mobile between 90 and 130 K (Ref. 58) and we observed the hysteresis effect only for temperatures above 100 K; (2) the activation energy that we measured in Sec. III corresponds well with what is expected for Zn interstitials; (3) for positive gate bias, the threshold moves to higher positive bias, which is consistent with positively charged Zn interstitials in an n-type semiconductor; and (4) this effect is observed in a helium environment where we do not expect any oxygen to be available for adsorption, especially since we are able to repeatedly cycle the effect. Presumably, the Zn interstitials remain within the physical ZnO nanoplate, although more research is needed to determine the location of the active conduction channel and how it is affected by the Zn interstitials. We note that alkali-metal ions could be introduced during typical semiconductor processing; however, we were careful to select chemical developers [methyl isobutyl ketone (MIBK) and acetone] that do not contain any metal ions. Additionally, energy dispersive spectroscopy measurements do not show any evidence of alkali metals.

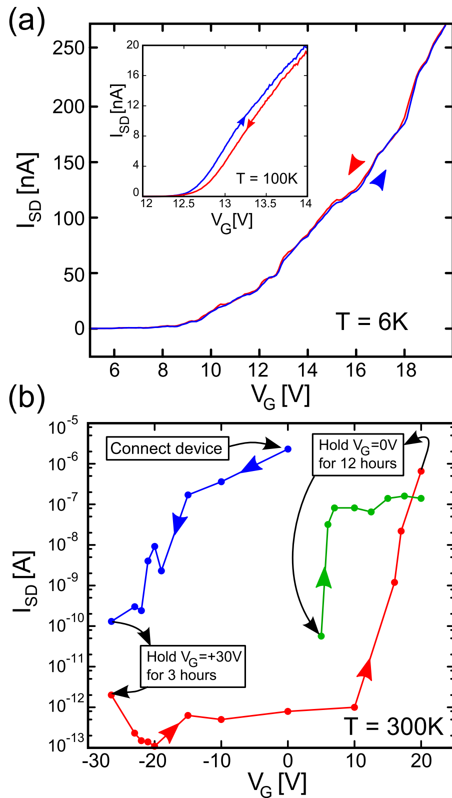

FIG. 6. (Color online) (a) Successive transconductance sweeps at 6 K, showing no hysteresis. This is contrasted by (inset) successive transconductance sweeps at 100 K for which hysteresis is evident. The effect is frozen out at temperatures below 100 K. (b) A sequence of transconductance sweeps at 300 K taken after holding V_G at different values. The threshold shifts by more than 30 V when V_G is held at +30 V for 3 h. We believe this is caused by mobile, positively charged Zn interstitials, as described in the text.

The fact that threshold voltage can be tuned over tens of volts may be of interest to device applications, as this behavior is both reversible and nonvolatile. However, as discussed earlier, this variable threshold also makes accurate determination of effective mobility to be difficult since V_T in Eq. (4) is constantly changing.

VII. CONCLUSION

In this paper, we present a comprehensive investigation into the electronic and magnetotransport properties of ZnO nanoplates grown by the VLS method. Unlike conventional nanostructures such as nanowires, the unique geometry of nanoplates allows us to conduct four-terminal van der Pauw and Hall-effect measurements. Using these techniques, we measure resistivity versus temperature and observe an activation energy (32 meV) characteristic of Zn interstitials that function as n-type donors. We report on magnetoresistance measurements showing weak localization in ZnO nanostructures and find the effect to be strongly dependent on temperature and only weakly dependent on carrier concentration. We obtain electron inelastic-scattering lifetimes by fitting magnetoresistance data to three-dimensional weak localization theory. We observe that the phase coherence lifetime scales as T^{-3}, characteristic of electron-phonon-scattering processes, and that the phase coherence length scales as $T^{-3/4}$ and is 50–100 nm at 1.9 K. We do not observe any evidence of antilocalization, suggesting that spin-orbit scattering is comparably weak and thus ZnO nanostructures may be useful for spintronic applications. Finally, we report on Hall mobility versus temperature and carrier concentration, finding a mobility of $\sim$100 cm^2/V s at 275 K, which is comparable to what is observed in ZnO thin films. We compare our calculated Hall mobility to the commonly reported field-effect mobility for nanowires and find that the field-effect mobility overestimates the Hall mobility by a factor of 2 in our devices but does function as a reasonable approximation. We comment on temperature-dependent hysteresis observed during transconductance measurements and attribute it to mobile, positively charged Zn interstitial impurities.

ACKNOWLEDGMENTS

This work was supported by NSF/NNIN through the use of their facilities at Harvard University's Center for Nanoscale Systems (CNS). The authors thank Warren Moberly-chan and David Bell for transmission electron microscopy work. E. M. L. recognizes support from the U. S. Department of Homeland Security.

*likovich@post.harvard.edu

[1] X. D. Wang, C. J. Summers, and Z. L. Wang, Nano Lett. **4**, 423 (2004).
[2] Y. C. Kong, D. P. Yu, B. Zhang, W. Fang, and S. Q. Feng, Appl. Phys. Lett. **78**, 407 (2001).
[3] P. D. Yang, H. Q. Yan, S. Mao, R. Russo, J. Johnson, R. Saykally, N. Morris, J. Pham, R. R. He, and H. J. Choi, Adv. Funct. Mater. **12**, 323 (2002).
[4] D. C. Look, D. C. Reynolds, C. W. Litton, R. L. Jones, D. B. Eason, and G. Cantwell, Appl. Phys. Lett. **81**, 1830 (2002).
[5] K.-K. Kim, H.-S. Kim, D.-K. Hwang, J.-H. Lim, and S.-J. Park, Appl. Phys. Lett. **83**, 63 (2003).
[6] B. Xiang, P. Wang, X. Zhang, S. A. Dayeh, D. P. R. Aplin, C. Soci, D. Yu, and D. Wang, Nano Lett. **7**, 323 (2007).
[7] Q. Wan, Q. H. Li, Y. J. Chen, T. H. Wang, X. L. He, J. P. Li, and C. L. Lin, Appl. Phys. Lett. **84**, 3654 (2004).
[8] K. Ueda, H. Tabata, and T. Kawaib, Appl. Phys. Lett. **79**, 988 (2001).
[9] L. Q. Liu, B. Xiang, X. Z. Zhang, Y. Zhang, and D. P. Yu, Appl. Phys. Lett. **88**, 063104 (2006).
[10] J. B. Cui and U. J. Gibson, Appl. Phys. Lett. **87**, 133108 (2005).
[11] M. H. Huang, S. Mao, H. Feick, H. Q. Yan, Y. Y. Wu, H. Kind, E. Weber, R. Russo, and P. D. Yang, Science **292**, 1897 (2001).
[12] M. Zimmler, J. Bao, F. Capasso, S. Muller, and C. Ronning, Appl. Phys. Lett. **93**, 051101 (2008).
[13] U. Özgür, Y. I. Alivov, C. Liu, A. Teke, M. A. Reshchikov, S.

Dogan, V. Avrutin, S.-J. Cho, and H. Morkoc, J. Appl. Phys. **98**, 041301 (2005).
[14] S. A. Wolf, D. D. Awschalom, R. A. Buhrman, J. M. Daughton, S. von Molnar, M. L. Roukes, A. Y. Chtchelkanova, and D. M. Treger, Science, **294**, 1488 (2001).
[15] I. Appelbaum, B. Huang, and D. J. Monsma, Nature (London) **447**, 295 (2007).
[16] Y. Ohno, D. K. Young, B. Beschoten, F. Matsukura, H. Ohno, and D. D. Awschalom, Nature (London) **402**, 790 (1999).
[17] K. Masuko, A. Ashida, T. Yoshimura, and N. Fujimura, J. Appl. Phys. **103**, 07D124 (2008).
[18] H. Yu, J. Li, R. A. Loomis, L.-W. Wang, and W. E. Buhro, Nature Mater. **2**, 517 (2003).
[19] Z. Fan, D. Wang, P.-C. Chang, W.-Y. Tseng, and J. G. Lu, Appl. Phys. Lett. **85**, 5923 (2004).
[20] Z. Fan, P.-C. Chang, J. G. Lu, E. C. Walter, R. M. Penner, C.-H. Lin, and H. P. Lee, Appl. Phys. Lett. **85**, 6128 (2004).
[21] Y. W. Heo, L. C. Tien, Y. Kwon, D. P. Norton, S. J. Pearton, B. S. Kang, and F. Ren, Appl. Phys. Lett. **85**, 2274 (2004).
[22] P.-C. Chang, Z. Fan, C.-J. Chien, D. Stichtenoth, C. Ronning, and J. G. Lu, Appl. Phys. Lett. **89**, 133113 (2006).
[23] J. Yoon, A. M. Girgis, I. Shalish, L. R. Ram-Mohan, and V. Narayanamurti, Appl. Phys. Lett. **94**, 142102 (2009).
[24] R. S. Wagner and W. C. Ellis, Appl. Phys. Lett. **4**, 89 (1964).
[25] P. A. Hu, Y. Q. Liu, L. Fu, X. B. Wang, and D. B. Zhu, Appl. Phys. A: Mater. Sci. Process. **80**, 35 (2005).
[26] B. Illy, B. A. Shollock, J. L. MacManus-Driscoll, and M. P. Ryan, Nanotechnology **16**, 320 (2005).
[27] E. W. Petersen, E. M. Likovich, K. J. Russell, and V. Narayanamurti, Nanotechnology **20**, 405603 (2009).
[28] M. A. Zimmler, T. Voss, C. Ronning, and F. Capasso, Appl. Phys. Lett. **94**, 241120 (2009).
[29] Z.-M. Liao, K.-J. Liu, J.-M. Zhang, J. Xu, and D.-P. Yu, Phys. Lett. A **367**, 207 (2007).
[30] L. J. van der Pauw, Philips Tech. Rev. **20**, 220 (1958).
[31] D. K. Schroder, *Semiconductor Material and Device Characterization*, 3rd ed. (Wiley-Interscience, Hoboken, NJ, 2006).
[32] H. J. Fritzsche, J. Phys. Chem. Solids **6**, 69 (1958).
[33] X. D. Liu, E. Y. Jiang, and Z. Q. Li, J. Appl. Phys. **102**, 073708 (2007).
[34] J. Goldberger, D. J. Sirbuly, M. Law, and P. Yang, J. Phys. Chem. B **109**, 9 (2005).
[35] D. C. Look, J. W. Hemsky, and J. R. Sizelove, Phys. Rev. Lett. **82**, 2552 (1999).
[36] G. Bergmann, Phys. Rep. **107**, 1 (1984).
[37] P. A. Lee and T. V. Ramakrishnan, Rev. Mod. Phys. **57**, 287 (1985).
[38] D. J. Bishop, R. C. Dynes, and D. C. Tsui, Phys. Rev. B **26**, 773 (1982).
[39] T. Andrearczyk, J. Jaroszynski, G. Grabecki, T. Dietl, T. Fukumura, and M. Kawasaki, Phys. Status Solidi C **3**, 1030 (2006).
[40] Q. Xu, L. Hartmann, H. Schmidt, H. Hochmuth, M. Lorenz, R. Schmidt-Grund, D. Spemann, A. Rahm, and M. Grundmann, Thin Solid Films **515**, 2549 (2006).
[41] S. Hikami, A. I. Larkin, and Y. Nagaoka, Prog. Theor. Phys. **63**, 707 (1980).
[42] A. Kawabata, Solid State Commun. **34**, 431 (1980).
[43] A. Kawabata, J. Phys. Soc. Jpn. **49**, 628 (1980).
[44] R. G. Mani, L. Ghenim, and J. B. Choi, Solid State Commun. **79**, 693 (1991).
[45] X. Z. Yu, Y. Yang, W. Pan, and W. Z. Shen, Appl. Phys. Lett. **92**, 092106 (2008).
[46] F. A. Lindholm and R. W. Ayres, Proc. IEEE **56**, 371 (1968).
[47] S. M. Sze and K. K. Ng, *Physics of Semiconductor Devices*, 3rd ed. (Wiley-Interscience, Hoboken, NJ, 2007).
[48] E. M. Kaidashev, M. Lorenz, H. von Wenckstern, A. Rahm, H. C. Semmelhack, K. H. Han, G. Benndorf, C. Bundesmann, H. Hochmuth, and M. Grundmann, Appl. Phys. Lett. **82**, 3901 (2003).
[49] H. Kato, M. Sano, K. Miyamoto, and T. Yao, Jpn. J. Appl. Phys., Part 1 **42**, 2241 (2003).
[50] K. Iwata, P. Fons, S. Niki, A. Yamada, K. Matsubara, K. Nakahara, and H. Takasu, Phys. Status Solidi A **180**, 287 (2000).
[51] N. W. Ashcroft and N. D. Mermin, *Solid State Physics* (Thomson Learning, New York, 1976).
[52] T. Edahiro, N. Fujimura, and T. Ito, J. Appl. Phys. **93**, 7673 (2003).
[53] A. R. Hutson, J. Phys. Chem. Solids **8**, 467 (1959).
[54] P. Wagner and R. Helbig, J. Phys. Chem. Solids **35**, 327 (1974).
[55] D. C. Look, D. C. Reynolds, J. R. Sizelove, R. L. Jones, C. W. Litton, G. Cantwell, and W. C. Harsch, Solid State Commun. **105**, 399 (1998).
[56] I. V. Markevich, V. I. Kushnirenko, L. V. Borkovska, and B. M. Bulakh, Solid State Commun. **136**, 475 (2005).
[57] B. T. Adekore, R. F. Davis, and D. W. Barlage, J. Appl. Phys. **101**, 024902 (2007).
[58] P. Erhart and K. Albe, Appl. Phys. Lett. **88**, 201918 (2006).